ROYAL SOCIETY
OF CHEMISTRY

PAPER

Digital and experimental design of CO_2-responsive polymers based on acrylamide monomers for carbon capture

Emil Pashayev [ID] and Prokopios Georgopanos [ID] *

This study provides a comprehensive evaluation of the CO_2 capture performance of the CO_2-responsive homopolymer poly(N-[3-(dimethylamino)propyl]-acrylamide) (PDMAPAm) and its diblock copolymer poly(N-[3-(dimethylamino)propyl]-acrylamide)-b-poly(methyl methacrylate) (PDMAPAm-b-PMMA), with a particular emphasis on their integration into membrane adsorbers for direct air capture (DAC) applications. A central novelty of this work is the development of a pioneering unified kinetic model that, for the first time, couples polymerization reaction kinetics with CO_2 adsorption kinetics. This model enables the digital predictive design of polymer materials whose CO_2 uptake is expressed directly as a function of polymer properties. By systematically varying the molar mass of the amine-functional PDMAPAm block and the poly(methyl methacrylate) (PMMA) content, this study identifies the optimal polymer properties that balance high CO_2 uptake with favorable processing characteristics. Adsorption experiments conducted under dry conditions revealed a physisorption-dominated mechanism, where CO_2 primarily interacts with tertiary amine and carbonyl functional groups. Notably, the unified model predicted a target molar mass of 18.5 kDa for the homopolymer of PDMAPAm and identified the optimal synthesis ratio of RAFT : initiator : monomer. This model also accurately forecasts the CO_2-uptake capacity of the PDMAPAm homopolymer to be 0.05 mmol g^{-1} and that of its corresponding diblock copolymer (PDMAPAm-b-PMMA) to be approximately 0.1 mmol g^{-1} under dry ambient conditions.

Introduction

Carbon capture technology is a key research field currently being developed for application[1] in various industries such as power generation,[2] chemical production,[3] and metal production plants[4] to reduce CO_2 emissions. In addition, due to the insufficient progress in industrial decarbonization, attention has shifted toward capturing atmospheric CO_2, even at a relatively low concentration, through an emerging approach known as direct air capture (DAC).

As mentioned before, DAC is designed to capture carbon dioxide (CO_2) directly from the atmosphere, addressing the urgent need to mitigate climate change.[5–10] This process involves the use of adsorbents, which are materials that can selectively capture and hold CO_2 molecules from the air.[6,11,12] The DAC process typically involves drawing ambient air into a system where it passes over an adsorbent material.[10,13] The CO_2 molecules are captured on the adsorbent surface through physical or chemical interactions.[10,13,14] This phenomenon is called adsorption. When the adsorbent becomes saturated with CO_2, it undergoes a regeneration process, which is called

desorption, often involving a temperature or pressure or electric swing, to release the captured CO_2 for storage or utilization.[15–17]

The development and optimization of adsorbents for DAC are crucial for improving the efficiency, energy costs and scalability of this technology.[6,18] By enhancing the CO_2 adsorption capacity and stability of these materials, researchers aim to make DAC a viable solution for large-scale carbon removal, contributing to global efforts to combat climate change.[11,12] Various adsorbent materials are utilized in DAC technologies to capture CO_2 directly from the atmosphere.[11,19–22] Among the various adsorbents, materials such as silica, alumina, zeolite 13X, and amine-functionalized adsorbents,[23,24] including polyethyleneimine (PEI), tetraethylenepentamine (TEPA), and diblock copolymers,[25,26] have shown significant promise. Recent studies have demonstrated that amine-functionalized adsorbents exhibit high CO_2 adsorption capacities and excellent cyclic stability, making them suitable for repeated use in DAC systems.[27] In particular, amine-containing polymers, such as polyethyleneimine (PEI) and tetraethylenepentamine (TEPA), have emerged as particularly promising adsorbents for DAC applications.[11,28–31]

Especially, amine-containing diblock copolymers exhibit an excellent performance in capturing CO_2, considering that the amine group has a strong affinity for CO_2.[25,26] In particular, diblock copolymers with amine-containing groups such as poly(2-

Helmholtz-Zentrum Hereon, Institute of Membrane Research, Max-Planck-Str. 1, 21502 Geesthacht, Germany. E-mail: prokopios.georgopanos@hereon.de

(dimethylamino)ethyl methacrylate) (PDMAEMA),[32–35] poly(*N,N*-dimethylallylamine) (PDMAAm),[36–39] poly(2-aminoethyl methacrylate) (PAEM),[40,41] and poly(*N*-[3-(dimethylamino)propyl]acrylamide) (PDMAPAm)[42] hold great potential to be used as adsorbents for DAC due to their high CO_2 reactivity, high CO_2 selectivity,[32,42,43] high porosity,[44–48] and scalability.[42,49–51] These polymers display advantageous properties ideal for CO_2 capture technologies, featuring a stable, relatively high, and swift CO_2 adsorption capacity, as well as a low desorption temperature.[51–53] The presence of an amine-containing group as a block on the surface and within the pore walls of diblock copolymers, together with their tunable properties *via* simulation, enables them to exhibit CO_2-responsive behavior. This allows for adjustable pore sizes and chemical surface interactions during CO_2 adsorption and desorption.

Unlike conventional amine-functionalized adsorbents such as primary or secondary amine-grafted silica, amine-impregnated porous supports and amine-modified carbons, which often suffer from oxidative degradation, pore blockage, amine leaching, and poor cyclic stability under humid or elevated-temperature DAC conditions,[54,55] CO_2-responsive diblock copolymers have potential to mitigate many of these issues. Because their amine groups are covalently built into the polymer backbone rather than physically dispersed or surface-grafted, these materials exhibit enhanced structural integrity and improved resistance to chemical and thermal degradation.[56] Moreover, the microphase separation inherent to diblock copolymers allows precise control over their domain morphology, facilitating the design of ordered nanoscale pathways for gas diffusion and providing tunable sorption–desorption kinetics, which are features not readily achievable in conventional amine-loaded sorbents.[57] These distinct advantages justify the exploration of CO_2-responsive diblock copolymers as next-generation adsorbents and highlight the rationale behind the material design adopted in this study. Apart from this, CO_2-responsive polymers offer significant potential for use in polymer–filler mixed-matrix membrane adsorbers, owing to their tunable affinity toward CO_2. Consequently, understanding their interactions with various fillers is critical. In previous publications,[51,58] PDMAPAm and PDMAPAm-*b*-PMMA polymers were coated onto PDMS (gutter layer) to prepare a thin-film composite membrane, which showed stable permeability and selectivity values for several cycles of time-lag measurements for different gases such as CO_2, O_2, N_2, and H_2. The interaction between the PDMAPAm chains and the underlying PDMS gutter layer can be attributed to a combination of physical adsorption, hydrogen bonding, and interfacial entanglement, all of which contribute to the stability and performance of the composite membrane.[59] Apart from PDMS, as fillers MOFs are also expected to show the strongest and most specific interactions with PDMAPAm-based polymers, primarily because these polymers contain amide and amine functional groups capable of coordinating directly with the open metal sites present in many CO_2-selective MOFs, forming strong Lewis acid–base or hydrogen-bonding interactions at the polymer–filler interface.[60] This coordination not only enhances interfacial adhesion but also increases the density of COs-affinitive sites, enabling synergistic

sorption-driven transport, which is highly compatible with the chemical nature of PDMAPAm.[61]

A detailed understanding of the CO_2 transport behavior in PDMAPAm- and PDMAPAm-*b*-PMMA-coated membranes as selective layers and its dependence on membrane morphology has been established in our previous studies.[51,58] These studies demonstrated that the CO_2/N_2 permeability selectivity of the membranes can reach values as high as 10–15, indicating that the polymers exhibit pronounced CO_2-responsive behavior.[51,58] The dense structure of these polymers was confirmed through SEM imaging, which reveals a continuous and nonporous selective layer, in which gas transport is dominated by polymer–gas interactions rather than convective flow.[51] In these dense polymer membranes, gas permeation follows the solution–diffusion mechanism, wherein gas molecules dissolve in the polymer matrix and subsequently diffuse through it.[62]

Recent reports on CO_2-responsive polymers have established key structure–property relationships that guide contemporary material design strategies.[63–65] Moreover, several studies have developed reaction kinetic models of RAFT polymerization to simulate polymer synthesis, enabling optimization of the polymer properties[50,66] and polymerization rate[50,67,68] and providing predictive tools for process upscaling.[67] Furthermore, some modeling efforts have focused on CO_2-adsorption isotherms in amine-based membrane adsorbers, offering valuable insights into their adsorption mechanisms and sorbent performance.[69–72] However, to date, no study has established a correlation between polymerization kinetics and the CO_2-adsorption behavior of the resulting polymer material. Building on this gap in the state of the art, we explicitly articulate the working hypothesis of the present study that CO_2 uptake by the PDMAPAm homopolymer and PDMAPAm-*b*-PMMA diblock copolymer can be rationally optimized by establishing a unified kinetic model that couples polymerization kinetics with CO_2 adsorption kinetics, thereby enabling predictive control over the polymer properties and its corresponding CO_2-capture performance.

Experimental

Material and methods

N-[3-(Dimethylamino)propyl]acrylamide (stabilized with MEHQ) (DMAPAm, >98.0%, TSI, Zwijndrecht, Belgium) was firstly dissolved in 1,4 dioxane (≥99.8%, Merck, Darmstadt, Germany) and percolated through a column of basic aluminum oxide (>98%, Sigma-Aldrich) prior to use to remove the inhibitor. Then, 2,2′-azobis(2-methylpropionitrile) (AIBN, 98%, Sigma-Aldrich, Taufkirchen, Germany, stored at 4 °C) and 4-cyano-4-[(dodecylsulfanylthiocarbonyl)-sulfanyl]pentanoic acid (CDTPA, 97%, Sigma-Aldrich, Taufkirchen, Germany, stored at 4 °C) were added to the monomer and solvent mixture. Methyl methacrylate (99%, stabilized with ≤30 ppm MEHQ, Sigma-Aldrich, Steinheim, Germany) was also freshly percolated using the same procedure for the same reason. Nitrogen was purchased from Air Liquide (Hamburg, Germany, 99.999% purity). The polymer was precipitated in *n*-hexane (99%, Sigma-Aldrich, Taufkirchen, Germany). Proton nuclear magnetic

resonance (¹H NMR) measurements were carried out in deuterated chloroform-d1 (CDCl$_3$, 99.8% containing 0.03% (v/v) TMS, Sigma-Aldrich, Taufkirchen, Germany, stored at 4 °C). Gel permeation chromatography (GPC) measurements were carried out in N,N-dimethyl acetamide (DMAc, ≥99.9%, Sigma-Aldrich, Taufkirchen, Germany).

Synthesis of PDMAPAm

For the synthesis of PDMAPAm *via* reversible addition–fragmentation chain transfer (RAFT) polymerization in a small lab flask, CDTPA (18.0 mg, 0.04 mmol, 0.7 eq.), AIBN (10.0 mg, 0.06 mmol, 1 eq.) and percolated DMAPAm (2000 mg, 13.00 mmol, 200 eq.) were dissolved in 9 mL of 1,4-dioxane (20 wt% monomer content). The mixture in the flasks was degassed with nitrogen in a cold-water bath at 15 °C for 20 minutes. Following this, polymerization was conducted in a 20 mL glass flask using a thermo-shaker set at 70 °C and 250 rpm for 4 hours. The reaction was terminated by exposing the reaction medium to air in an ice bath (0 °C). Samples for (¹H) NMR and GPC were taken to determine the monomer conversion (90%) and molecular weight of the synthesized polymer, respectively. The final product was precipitated from n-hexane, filtered, and dried overnight in a vacuum oven at 35 °C under 1 mbar.

Synthesis of PDMAPAm-b-PMMA

To synthesize the PDMAPAm-b-PMMA diblock copolymer, dried PDMAPAm (1000 mg, 0.03 mmol, 2 eq.), which served as the macro-RAFT/macro-stabilizer agent, MMA (480 mg, 4.8 mmol, 165 eq.), and AIBN (5 mg, 0.03 mmol, 1 eq.) were dissolved in 6 mL of 1,4-dioxane. The mixture was degassed with nitrogen in a cold-water bath at 15 °C for 20 minutes. Then polymerization was conducted in a 10 mL glass flask using a thermo-shaker at 70 °C and 250 rpm for 24 hours. The reaction was terminated by exposing the medium to air in an ice bath (0 °C). Samples for ¹H NMR and GPC were taken to determine the MMA conversion (92%) and the molecular weight of the synthesized diblock copolymer, respectively. The polymer was precipitated in n-hexane and dried in a vacuum oven at 35 °C and 1 mbar for 24 hours (see the detailed synthesis protocol in Tables S1 and S2 and properties of both the homopolymer and diblock copolymer in Table S3 and Fig. S1 in the SI).

The synthesis protocol for PMMA$_{70}$ can be found in a previous publication,[49] while the polymer properties are given in Table S4 in the SI.

Characterization

Gas permeation chromatography (GPC)

The apparent molecular weight distributions of the PDMAPAm homopolymers (macro-RAFT agents) and PDMAPAm-b-PMMA diblock copolymers were measured by GPC at 50 °C using DMAc with added lithium chloride (0.1 M) as the eluent. A Waters 717 Plus instrument (Waters, Milford, MA, USA) equipped with PSS GRAM columns (PSS GmbH, Mainz, Germany) [GRAM precolumn (dimensions of 8–50 nm) and two GRAM columns of

different porosity (3000 and 1000)] with dimensions of 8 × 300 mm and a particle size of 10 μm was used. The samples were measured at a flow rate of 1 mL min^{-1} using a VWR-Hitachi 2130 pump (VWR Hitachi, Darmstadt, Germany) and a VWR-Hitachi L2490 RI (refractive index) detector (VWR Hitachi, Darmstadt, Germany). The GPC was calibrated with narrow PMMA standards and data were analyzed using the PSS WinGPC UniChrom software (PSS GmbH, Mainz, Germany).

Proton nuclear magnetic resonance (¹H NMR)

¹H NMR spectroscopy experiments were performed using a Bruker AV500 spectrometer (Bruker, Rheinstetten, Germany) and a Spinsolve Carbon 80 Ultra MultiX benchtop spectrometer (80 MHz, Magritek GmbH, Aachen, Germany). Spectra were recorded with the Bruker AV500 spectrometer by applying a 10 ms 90° pulse at a sample temperature of 298 K. 16 scans were recorded with a relaxation delay of 3 s. Similarly, the experiments with the Spinsolve Carbon 80 Ultra MultiX spectrometer were performed using the Proton$^+$ protocol with 4 scans, an acquisition time of 6.4 s, a repetition time of 1 min, and a pulse angle of 90°. The sample concentration was 20 g L^{-1}, and CDCl$_3$ was employed as the solvent. The ¹H NMR spectra were analyzed with the MestReNova 15.1 software (Mestrelab Research, Santiago de Compostela, Spain). 1,3,6-Trioxane was used as an internal standard. DMAPAm conversion from macro-RAFT synthesis was estimated by comparing the integration of the double-bond proton areas in the spectra of the sample before and after the reaction, yielding a conversion of 92%. Using the same method,[51] the conversion of methyl methacrylate in the second block synthesis, also measured in CDCl$_3$, was calculated from the decrease in the integral of the monomer peaks, which was 91%.

High-pressure differential scanning calorimetry (DSC)

The change in the glass transition temperature of the PDMAPAm homopolymer was examined using high-pressure differential scanning calorimetry in CO$_2$- and N$_2$-containing environments at different pressures. A High-Pressure DSC 1 from Mettler Toledo was used to investigate the in situ thermal transitions of PDMAPAm. The measurements were conducted at 1, 3, 5, and 7 bar in a CO$_2$-containing environment, whereas the measurements under nitrogen were performed only at a pressure of 1 bar. The temperature program for the HP-DSC measurements consists of two steps. Firstly, the sample was heated from 30 °C to 120 °C, held at 120 °C for 5 minutes to establish an isotherm, and then cooled back to 20 °C. In the second step, the glass transition temperature (T_g) of the sample at each pressure is determined by heating the sample to 20 °C for 2 hours, saturating it with CO$_2$, and then increasing the temperature to 60 °C at 2 °C min^{-1}. When pressure was not applied, the temperature increase rate was set to 10 °C min^{-1}.

Magnetic suspension balance

The gravimetric sorption method was employed to study the sorption of dry carbon dioxide using a Rubotherm magnetic suspension balance (Rubotherm Präzisionsmesstechnik

GmbH, Bochum, now TA Instruments). The magnetic suspension balance enables precise measurement of the changes in force and mass on samples within controlled environments (such as pressure and temperature). These measurements facilitate the accurate determination of transport and state quantities (such as sorption and diffusion) and enable the investigation of chemical reactions (such as corrosion, coating, and drying). The holder remains suspended by a permanent magnet. The system allows for the measurement of weight changes in the holder and sample under varying pressure and temperature conditions. These changes can be linked to the specific gas uptake.[73–75] During adsorption experiments, the gas is introduced stepwise at controlled pressure and temperature, and the balance records the increase in sample weight until equilibrium is reached in each step. For desorption, the pressure is gradually reduced, and the decrease in weight is monitored to determine the release of gas from the material. The graph of specific gas uptake at a constant temperature *versus* pressure is known as the sorption isotherm of the gas for the material. To minimize disturbances caused by non-ideal behavior, it is preferable to consider the real gas density rather than the ideal gas density for the evaluation of the results.[73] A detailed description is provided in the literature.[73]

Results and discussion

For the synthesis of the PDMAPAm-*b*-PMMA diblock copolymer, the block lengths were intentionally selected to balance two essential requirements: (1) maintaining a high fraction of CO_2-responsive tertiary amine groups to ensure strong gas–polymer interactions and (2) incorporating a PMMA block of sufficient size to provide the mechanical integrity necessary for membrane formation.

The reaction conditions and composition used for synthesizing PDMAPAm and PDMAPAm-*b*-PMMA were selected based on established RAFT polymerization principles and prior publications on the RAFT polymerization of amine-containing monomers.[76–78] Specifically, the monomer-to-RAFT-agent and initiator ratios were chosen to ensure controlled radical polymerization with a narrow dispersity, following the common approach of maintaining an initiator-to-monomer ratio (AIBN : DMAPAm) of approximately 1 : 200 (ref. 51, 76 and 78) to achieve moderate polymerization rates and high end-group fidelity.[67] High end-group fidelity is very important for further chain growth with MMA during the synthesis of diblock copolymers.[79]

Our synthesis strategy began with the preparation of the PDMAPAm homopolymer, followed by chain extension with incrementally increasing PMMA block lengths. This stepwise approach allowed us to identify the range in which the diblock copolymer remained both mechanically stable and highly CO_2-responsive.

After that, the synthesized polymers, PDMAPAm and its diblock copolymer, PDMAPAm-*b*-PMMA, were systematically characterized to evaluate their interactions with CO_2 under dry conditions. Comparative analyses were conducted using PDMAPAm homopolymers with two distinct molar masses, as well as PDMAPAm-*b*-PMMA copolymers featuring a constant PDMAPAm block and varying PMMA block lengths. To accurately assess CO_2 adsorption behavior, the gas was treated as a real gas, and its density was calculated using the real gas equation of state.

Mechanism of dry CO_2 adsorption

Generally, the developed amine-based homopolymer, PDMAPAm, and diblock copolymer, PDMAPAm-*b*-PMMA, as shown in Fig. 1, can undergo physisorption when they interact with dry CO_2.

Dry CO_2 physisorption mechanism on PDMAPAm

As represented in Fig. 1(a), PDMAPAm has amide groups (consisting of carbonyl and secondary amine groups) and tertiary amine groups in its structure. When the PDMAPAm powder is exposed to dry CO_2, it is expected that its amide and tertiary amine groups can show affinity for CO_2.[80,81] Since the concentration of RAFT end groups is less than the concentration of functional groups on monomeric units, the interaction of the RAFT end groups with dry CO_2 is neglected.

Polyamides feature polar interaction sites, specifically (–NH) and (C=O) groups. A strong Lewis acid–base interaction occurs between CO_2 and the oxygen of the amide carbonyl. Polyamide-based materials such as melamine-based porous organic amide polymers capture 0.1 mmol per g CO_2 under dry conditions at P of 1 bar and T of 25 °C.[82] As for the tertiary amine group, it interacts with dry CO_2 only *via* one of the van der Waals interaction types,[65,66] which may be achieved due to the temporary dipoles created by fluctuations in the electron density over the CO_2 molecule and polarization of the tertiary amine group.[83]

Dry CO_2 physisorption mechanism on PMMA

Besides PDMAPAm, the PDMAPAm-*b*-PMMA diblock copolymer has a PMMA block in it structure, as shown in Fig. 1(b). Poly(methyl methacrylate) (PMMA) was thoroughly examined by Wissinger[84,85] because of its swelling and adsorption characteristics. These analyses demonstrate its outstanding adsorption behavior across various CO_2 pressures (0.1–10 MPa) and good swelling abilities,[84,86–88] indicating the strong interaction between PMMA and carbon dioxide compared to other polymers.[89,90] The interaction between the polymer side chains (containing methyl ester groups) and CO_2 was examined using various techniques, including *ab initio* calculations, FT-IR spectroscopy, and Raman spectroscopy. These analyses
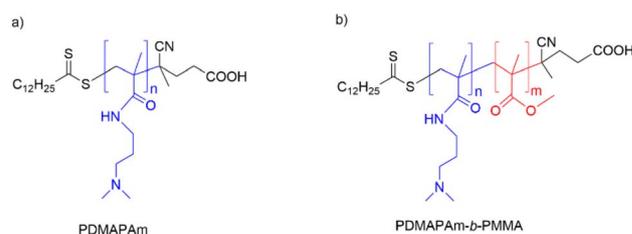

Fig. 1 Chemical structure of the RAFT-polymerized (a) homopolymer PDMAPAm and (b) diblock copolymer PDMAPAm-*b*-PMMA.

demonstrated that the carbonyl group participates in a Lewis acid–base interaction with CO_2,[91–97] which means that the attachment of CO_2 to PMMA is based on the interaction between the lone pairs of oxygen in the carbonyl groups of the polymer and the dipole moments of carbon dioxide.[91–97] In the context of CO_2 and PMMA, the oxygen in the carbonyl group acts as a Lewis base, donating an electron pair to the CO_2 molecule, which acts as a Lewis acid.

Dry CO_2 adsorption measurement

Several adsorption measurements were conducted to analyse the dry CO_2 capture performance of the synthesized CO_2-responsive polymer in a gravimetric adsorption device, as presented in Fig. 2.

Fig. 2 illustrates the CO_2 uptake capacity of the PMMA homopolymer, PDMAPAm homopolymer, and PDMAPAm-*b*-PMMA diblock copolymer at varying PMMA block contents, adsorption temperatures and molar masses. This is clear from the curves that both the homopolymer and diblock copolymer adsorb dry CO_2 and the CO_2 uptake capacity changes with the molar mass of the homopolymer, temperature and block content of the diblock copolymer. Another important point is that the CO_2 uptake of the homopolymers increases up to 6 bar, and then becomes constant, whereas a plateau appears at a higher pressure. As shown by the results for dry CO_2 adsorption, PDMAPAm captures 0.05 mmol g^{-1} under dry conditions at atmospheric pressure and 25 °C. This uptake capacity is very close to the CO_2 capture capacity of tertiary-amine-based polymer[98,99] and poly(amide)-based adsorbents, in which the interaction between CO_2 and the tertiary amine groups occurs *via* van der Waals forces[98–100] and the interactions between CO_2 and –NH or C=O groups occur based on Lewis acid–base interactions,[82] respectively. This indicates that CO_2 adsorption under dry conditions also occurred *via* identical interactions because PDMAPAm has both functional groups in its structure. Based on DFT studies,[101,102] tertiary amine has stronger interaction energy with CO_2, which is up to −16 kcal mol^{-1},[80,103,104] than amide, which changes between −5 and −10 kcal mol^{-1}.[81] Due to the stronger interaction energy between tertiary amines and dry

CO_2 compared to amide groups, CO_2 molecules are more likely to be retained near the tertiary amine sites. This leads to a higher local concentration and enhanced uptake of CO_2. Therefore, in this study, it is assumed that the CO_2 adsorption capacity of the PDMAPAm polymer, whose monomeric unit contains both a tertiary amine and an amide group, primarily arises from the interaction between dry CO_2 and its tertiary amine functionality.

Effect of molar mass on CO_2 capture

As is clear in Fig. 2, the CO_2 capture capacity of the PDMAPAm homopolymer increases very slightly as its molar mass increases. This trend can be attributed to the higher number of amine groups per mole in the polymer with a greater molar mass, which are the primary sites for CO_2 interaction, as reported previously.[51] Additionally, longer chain lengths may provide more free volume for CO_2 molecules.[105,106] However, the increase remains small because under dry conditions, the lone pair electrons on the nitrogen of the tertiary amine are sterically hindered by two methyl groups, limiting their interaction with CO_2.[94–97] Consequently, even as the number of amine groups increases, steric hindrance restricts their accessibility, resulting in only a minor improvement in uptake capacity.

Effect of PMMA content on CO_2 capture

Furthermore, Fig. 2 shows that the CO_2 adsorption capacity of the polymer increases with an increasing PMMA block portion in the diblock copolymer.

This is also clearly seen in the CO_2 adsorption capacity of PMMA as a homopolymer. The PMMA block can physically interact with CO_2 and this interaction is primarily through physical adsorption, where CO_2 molecules diffuse into the polymer matrix.[107] The CO_2 uptake capacity of the PMMA homopolymer reaches 0.1 mmol g^{-1} at 1 bar and 30 °C, which is very close to the value mentioned in the literature.[107] As mentioned before, these interactions between CO_2 and PMMA are described as Lewis acid–base interactions involving the transfer of electron pairs, resulting in strong, stable bonds.[108] Higher pressure reduces the free volume, facilitating electron-pair transfer and strengthening the interaction.[108] This results in a more efficient and higher CO_2 uptake capacity. However, the interactions between PDMAPAm and CO_2 are due to temporary dipoles created by fluctuations in electron density,[83] and while an increasing pressure brings the molecules closer together, enhancing these transient dipoles, the interactions remain weaker and less specific compared to Lewis acid–base interactions.[83] Therefore, the CO_2 uptake capacity increases more significantly with pressure through Lewis acid–base interactions due to their stronger and more stable nature.

DFT findings show that the interaction energy between CO_2 and the tertiary amine groups in PDMAPAm[65] is three-times more than the interaction energy between CO_2 and the oxygen of the carbonyl group in PMMA under dry conditions. This could be attributed to the fact that PDMAPAm has a greater CO_2 uptake capacity than PMMA;[109] however, this is not the case. Under dry conditions, the free electrons of the nitrogen in the
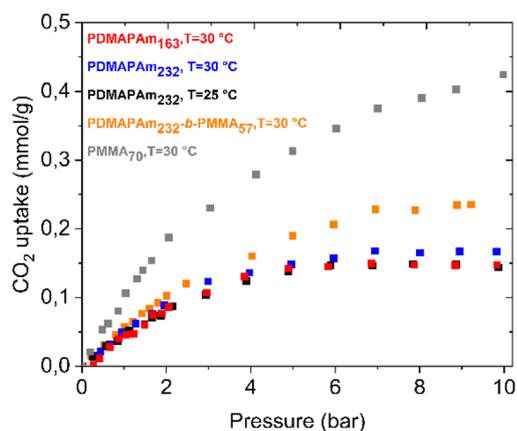

Fig. 2 CO_2 adsorption curves of PDMAPAm at different temperatures and molar masses compared with PMMA and PDMAPAm-*b*-PMMA.

tertiary amine groups of PDMAPAm are hindered by two methyl groups, and thus, the electrons of the tertiary amine groups cannot interact easily with CO_2.[54,110–112] However, the free electrons of the oxygen atoms of the carbonyl groups in the PMMA block are easily accessible to CO_2, which indicates that these electrons are not hindered and the ester group provides very attractive interaction sites for CO_2 molecules.[113,114] This could explain the increase in the CO_2 uptake capacity of the diblock copolymer with a PMMA block.

Effect of temperature on CO₂ capture

Another consideration is that Fig. 2 explains the effect of adsorption temperature on the CO_2 uptake capacity of the PDMAPAm homopolymer. The adsorption measurements with PDMAPAm were conducted at 25 °C and 30 °C because this interval reflects the typical ambient conditions at locations where DAC units are most likely to operate.[115,116] It can be clearly seen that a higher temperature leads to a higher CO_2 uptake capacity of the polymer, which was also mentioned in other publications,[117] but the effect of temperature is not significantly high.

Apart from this, 30 °C is very close to the glass transition temperature of the $PDMAPAm_{257}$ polymer at 1 bar if it is exposed to CO_2 (see Fig. 7). Therefore, above this temperature, it is possible that the CO_2 adsorption capacity of PDMAPAm will not increase any further.

Simulation of dry CO₂ physisorption model

To understand the kinetic mechanism of CO_2 adsorption on the polymers, the CO_2 adsorption isotherms of both the homopolymer and diblock copolymer were fit to two different adsorption models, the Langmuir and Freundlich models. The Langmuir and the Freundlich isotherm models were selected for fitting the CO_2 adsorption data due to their widespread applicability and theoretical relevance. These models have been extensively validated in the literature for similar systems.[14,118–122] Fig. 3 shows the results of the fitting of the experimental CO_2 uptake

Fig. 3 Kinetic model fitting for CO_2 physisorption on the PDMAPAm and PMMA homopolymers and the PDMAPAm-*b*-PMMA diblock copolymer.

values at different pressures to the Langmuir and Freundlich isotherm models.

It can be clearly seen from the fitting that the isotherms of both PDMAPAm and PDMAPAm-*b*-PMMA have a better fit with the Langmuir model than the Freundlich model. In particular, up to 7 bar, there is a good overlap between the simulated and experimental CO_2 adsorption isotherms for both the homopolymer and diblock copolymer, but the model deviates from the data thereafter. The reason for the deviation is that the glass transition temperature of the PDMAPAm polymer decreases as it is exposed to dry CO_2 at higher pressure, as shown in Fig. 7. Alternatively, when the PDMAPAm polymer is exposed to dry CO_2 at this temperature and above 5 bar, it is no longer in a glassy state. Therefore, the adsorption no longer follows the Langmuir model.

The Langmuir model indicates that monolayer adsorption occurs at homogeneous sites on both PDMAPAm and PDMA-PAm-*b*-PMMA.[14] This model posits that the solid surface has a specific number of active sites, each capable of adsorbing only one adsorbate molecule (CO_2). Equilibrium is reached when all these active sites are occupied by CO_2 molecules, forming a monomolecular layer.[123,124] Essentially, the Langmuir isotherm describes a gradual progression towards maximum adsorption, resulting in a monomolecular layer that completely covers the solid surface of both PDMAPAm and PDMAPAm-*b*-PMMA. The Langmuir model also assumes that the CO_2 molecules adsorbed on the surface of the polymer material do not interact with each other, and the heat of adsorption is constant and independent of the degree of surface coverage.[125,126]

Moreover, from the fitting, the kinetic parameters of the Langmuir model, which are the equilibrium coefficient (k_L) and the maximum CO_2 capture capacity of the polymer (q_{max}), were estimated. With a variation in the molar mass of PDMAPAm, temperature, and the PMMA block content, the changes in the kinetic parameters of the Langmuir model were analysed, as shown in Fig. 4(a)–(c), respectively.

It can clearly be seen in Fig. 4 that as the molar mass of PDMAPAm, PMMA content, and adsorption temperature increase, q_{max} rises and k_L decreases simultaneously. Particularly, in Fig. 4(b), the effect of PMMA block content on both kinetic parameters is larger than the effect of the molar mass of PDMAPAm in Fig. 4(a) and the adsorption temperature in Fig. 4(c). The mild dependence of adsorption on temperature and molar mass is consistent with the dominant solution–diffusion mechanism in dense polymer matrices, where gas solubility and free volume govern sorption, as described in the classical membrane-science literature.[59,127] As shown in Fig. 4(b), the copolymers with larger hydrophobic PMMA domains exhibit higher adsorption capacities (q_{max}). This behavior is consistent with the role of PMMA in enhancing the polymer packing density and microphase-separated domain ordering, which promotes more accessible sorption pathways.[128,129] This is supported by studies showing that PMMA blocks act as apolar segments driving the formation of well-defined, compact microphase-separated structures in block copolymers, where PMMA-rich domains increase structural ordering and influence transport pathways.[128,130,131] At the same
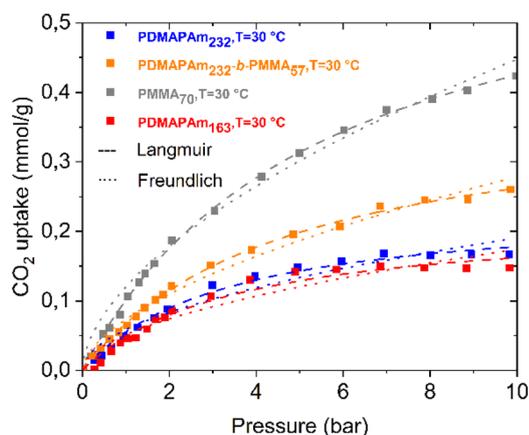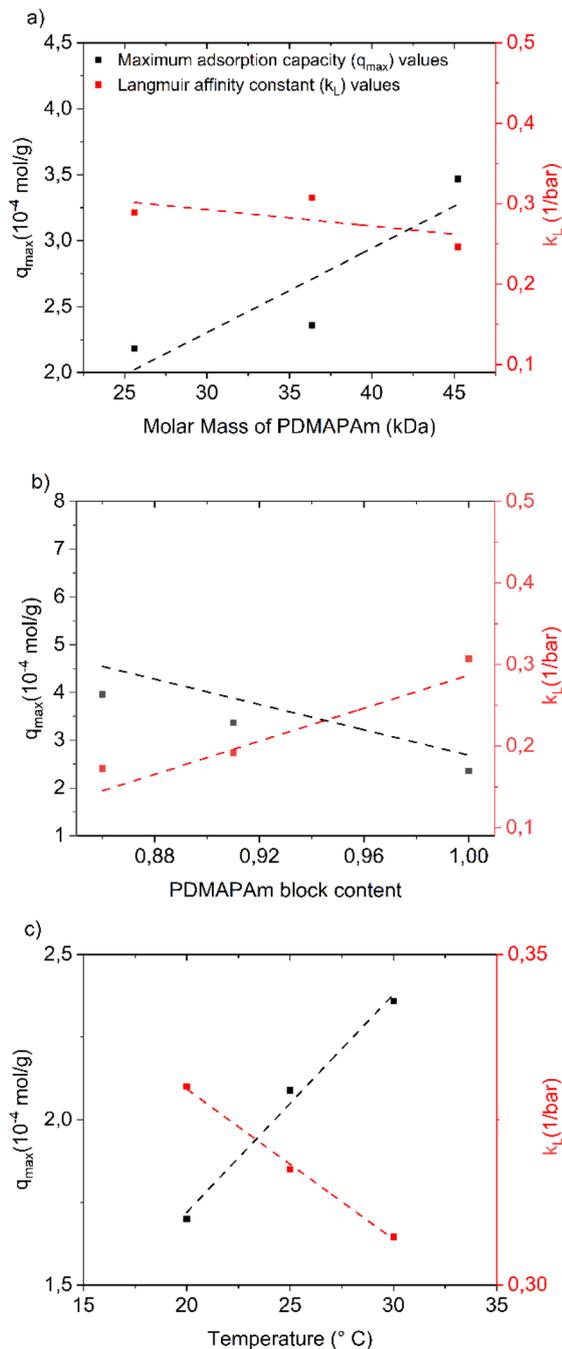
Fig. 4 Effect of the molar mass of PDMAPAm, the PMMA block and the adsorption temperature on the equilibrium coefficient and maximum CO_2 capture capacity of the polymer. Change in the kinetic parameters (q_{max} and k_L) of the Langmuir model with the (a) molar mass of homopolymer (PDMAPAm), (b) PDMAPAm block content of the diblock copolymer and (c) temperature.

time, DFT results show that CO_2 interacts with the tertiary amine groups[65] in PDMAPAm about three-times more strongly than with the carbonyl oxygen[109] in PMMA under dry conditions. Regardless, PDMAPAm does not exhibit higher CO_2 uptake. This is likely because the nitrogen lone pair in the tertiary amine is sterically hindered by two methyl groups, limiting its ability to bind CO_2.[61,110–112] In contrast, the carbonyl

oxygen in PMMA is more accessible, providing attractive interaction sites for CO_2. This accessibility may explain why adding a PMMA block increases the CO_2 uptake in the diblock copolymer.[113,114]

These effects of the polymer properties (molar mass of PDMAPAm and PMMA block content) and adsorption process variables (such as temperature and pressure in this case) on the kinetic parameters of the adsorption model can be used as an important bridge to combine polymer properties (which are mainly controlled by the polymerization kinetics[42,50,67]) with the adsorption behavior of the polymer.

Correlations between the surface and structural features of membrane materials and their performance arise from how the polymer morphology, free volume, and segmental mobility govern the gas diffusion pathways.[132] Surface heterogeneity and the distribution of functional groups strongly affect sorption behavior by modulating the gas–polymer interactions on the molecular scale.[132] Variations in chain packing density and local rigidity further determine the balance between diffusivity and solubility, thereby linking structural features directly to permeability and adsorption capacity.[133] In block-copolymer-based or nanostructured membrane adsorbers, microphase-separated domains create selective transport channels, highlighting the importance of tailoring their structural architecture to enhance both uptake and selectivity.[134]

Desorption of CO_2

In addition to evaluating the CO_2 adsorption behavior of the PDMAPAm homopolymer and the PDMAPAm-*b*-PMMA diblock copolymer, the desorption process was investigated under dry conditions, and the corresponding results are presented in Fig. 5.

Fig. 5 illustrates the CO_2 adsorption and desorption isotherms of the PDMAPAm homopolymer and PDMAPAm-*b*-PMMA diblock copolymer. It can be clearly seen that the copolymer adsorbs more CO_2 than the homopolymer, as mentioned before in the previous section. Additionally,
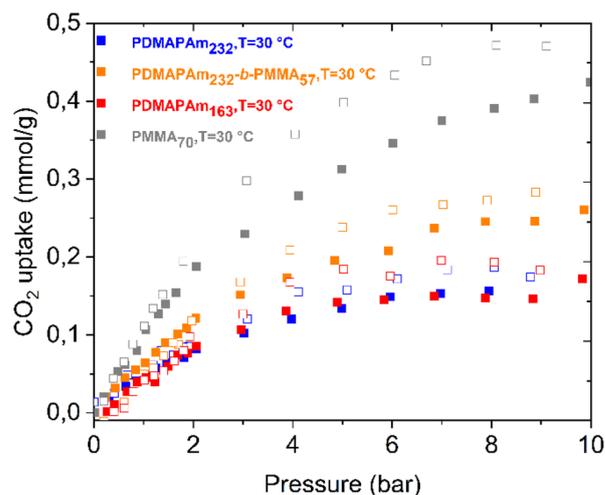

Fig. 5 CO_2 adsorption–desorption isotherms of PDMAPAm homopolymers with different molar masses, PMMA, and the PDMAPAm-*b*-PMMA diblock copolymer.

hysteresis is observed between the adsorption and desorption isotherms of both the homopolymer and diblock copolymer. The isotherms of polymers were measured in powder form, and the desorption isotherms were higher than the sorption isotherms for both PDMAPAm and PDMAPAm-*b*-PMMA, indicating a notable hysteresis effect in the sorption-desorption process. This phenomenon can be attributed to either the trapping effect caused by the interaction of CO_2 with the polymer or structural rearrangements. The hysteresis effect suggests that the sorbent/sorbate system is in a metastable state, and as pressure decreases, the gas is not released as readily as expected based on the thermodynamic equilibrium values.[82] In detail, PMMA exhibits greater CO_2 sorption hysteresis than PDMAPAm due to its glassy nature, which can lead to irreversible structural rearrangements and physical aging during desorption. The dual-mode sorption behavior and higher free volume in PMMA contribute to CO_2 entrapment,[135,136] whereas the more flexible and less glassy PDMAPAm allows for more reversible adsorption–desorption cycles.[51,58]

Cycling experiment

Since the polymers can also potentially be applied for long-term repeated adsorption–desorption processes in direct air capture technologies, it is very important to check their stability after several cycles of adsorption–desorption.

In this part, five cycles of dry CO_2 adsorption measurements were conducted at 1 bar and 30 °C for 1 h, whereas desorption was also performed for 1 h at 30 °C but under vacuum (0.001 bar). The multi-cycle performance of $PDMAPAm_{232}$ and $PDMAPAm_{232}$-*b*-$PMMA_{57}$ is illustrated in Fig. 6(a) and (b), respectively.

Fig. 6 shows that both $PDMAPAm_{232}$ and $PDMAPAm_{232}$-*b*-$PMMA_{57}$ exhibited a stable CO_2 uptake performance with very small fluctuations. The most crucial point is that both polymers maintained almost stable CO_2 uptake capacities with the number of cycles. This might be related to the fact that both polymers interact with dry CO_2 physically and do not form a chemical bond during adsorption, and therefore, the desorption process was performed at the same temperature as adsorption but at a pressure close to zero bar. This does not compromise the stability of the polymers, allowing them to be used for a long time after several cycles of adsorption–desorption.

Another important point is that both PDMAPAm and PDMAPAm-*b*-PMMA show very small hysteresis in the adsorption–desorption cycles, and the hysteresis fluctuates in each cycle. As mentioned before, the reason for the hysteresis is not due to the formation of chemical bonds but may be because the dry CO_2, which was adsorbed, chose a different pathway during desorption than during adsorption.

High-pressure DSC

Furthermore, DSC analysis under N_2 at 1 bar, as well as high-pressure DSC analysis with CO_2 supplied at varying pressures, were conducted to monitor the change in the glass transition temperature of PDMAPAm. These measurements were performed with respect to both the molar mass of the
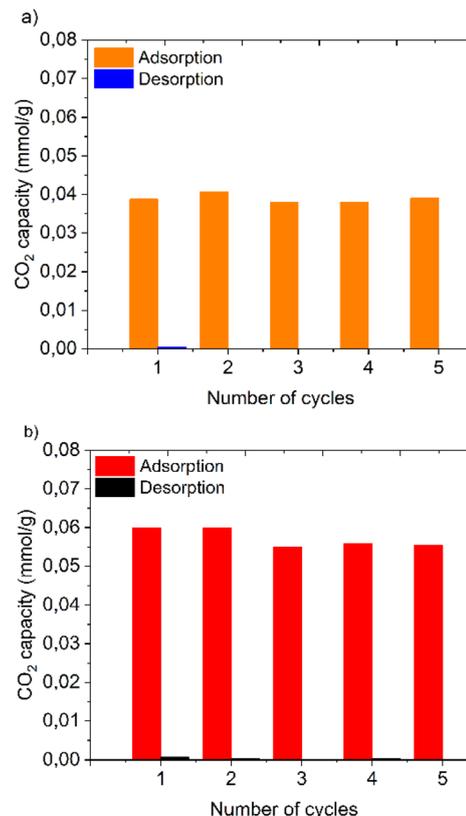

Fig. 6 Change in CO_2 uptake capacity of the polymer with the number of cycles. Adsorption–desorption cycling experiment on (a) $PDMAPAm_{232}$ and (b) $PDMAPAm_{232}$-*b*-$PMMA_{57}$ at 1 bar and 30 °C.

homopolymer and the CO_2 exposure pressure, and the results are presented in Fig. 7.

Fig. 7(a) shows the glass transition temperatures (T_g) of $PDMAPAm_{167}$ and $PDMAPAm_{232}$ exposed to CO_2 at different pressures, whereas Fig. 7(b) compares the glass transition temperatures of CO_2-exposed PDMAPAm with that of N_2-exposed PDMAPAm at different molar masses. It can be clearly seen that the T_g of the CO_2-exposed polymer is less than the T_g of the N_2-exposed polymer.

It is also crucial to note that the T_g of the N_2-exposed PDMAPAm increases with the molar mass of the polymer, whereas the trend is reciprocal for the CO_2-exposed PDMAPAm at 1 bar. As the molar mass of the polymer increases, the T_g of the N_2-exposed polymer increases, whereas the T_g of the CO_2-exposed polymer decreases, which means that the polymer interacts with CO_2 differently than with N_2. When PDMAPAm is exposed to dry CO_2, the CO_2 molecule physically interacts with the tertiary amine and amide groups of the polymer and attaches to them, and this interaction induces a plasticizing effect. These interactions reduce the intermolecular forces and increase the free volume within the polymer matrix, thereby enhancing the chain mobility and lowering the T_g.[54,104] Another point is that PDMAPAm with a higher molar mass interacts with CO_2 more. This trend totally agrees with the increasing trend of CO_2 capture capacity with the molar mass of the polymer, as also mentioned before and demonstrated in Fig. 2. Another
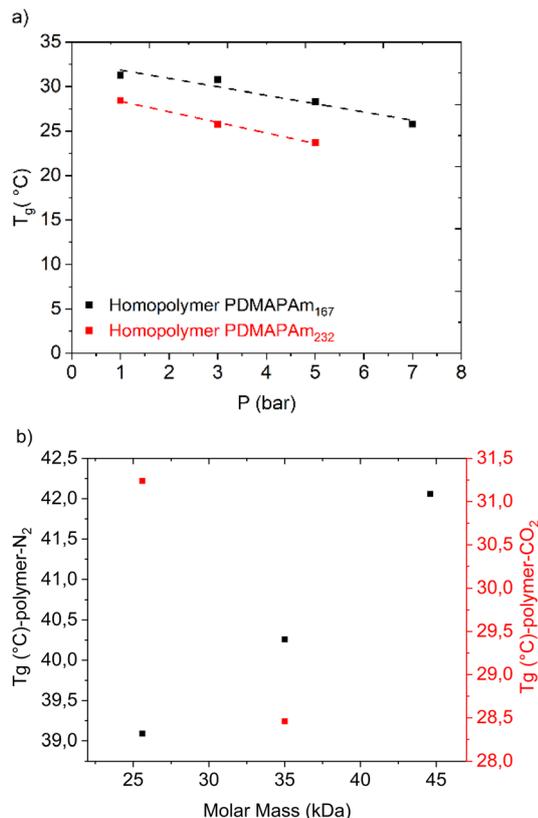
Fig. 7 (a) Change in glass transition temperature of CO_2-exposed PDMAPAm with two different molar masses at different pressures. (b) Comparison of change in glass transition temperature of CO_2-exposed PDMAPAm with N_2-exposed PDMAPAm at different molar masses.

consideration is that the slope of the trend line of T_g change with pressure for the CO_2-exposed polymer is almost the same as that for both homopolymers at different molar masses in the range of 1 bar to 7 bar.

Combination of kinetics for polymer synthesis with kinetics of physisorption (unified model)

To combine the polymerization kinetics[67] with adsorption kinetics, the following case study is applied: the aim was to synthesize a homopolymer, PDMAPAm$_{163}$, and its corresponding diblock copolymer, PDMAPAm$_{163}$-b-PMMA$_{30}$, and to simulate the adsorption behaviour of both the PDMAPAm$_{163}$ homopolymer and PDMAPAm$_{163}$-b-PMMA$_{30}$ diblock copolymer considering physisorption phenomena.

The kinetic model developed for the RAFT polymerization of dimethylaminopropylacrylamide (DMAPAm) is applied here to simulate the optimal synthesis recipe. The simulation showed that the optimal recipe for homopolymer (PDMAPAm) synthesis is RAFT : initiator : monomer ratio of 1.2 : 1 : 200 and at the same time, the model predicted the evolution of DMAPAm monomer conversion, number average molar mass and livingness of PDMAPAm for further chain extension with MMA to synthesize the PDMAPAm-b-PMMA diblock copolymer. The experiments for the synthesis of the homopolymer and diblock

copolymer, PDMAPAm-b-PMMA, were conducted using the predicted optimal recipe to test whether the kinetic model for polymer synthesis is correct. The comparison between the simulation and experimental results is shown in Fig. 8, and the molar mass characterization results for PDMAPAm and PDMAPAm-b-PMMA are shown in Table 1.

As can be clearly seen in Fig. 8 and Table 1, the kinetic model predicts the DMAPAm conversion, number-average molar mass, and livingness of PDMAPAm$_{163}$ quite well, as evidenced by the good agreement between the simulated and experimental data.

The dry CO_2 physisorption isotherm of the PDMAPAm$_{163}$-b-PMMA$_{30}$ polymer was simulated using the results from Fig. 4. Interpolation (also assuming that this adsorption follows the
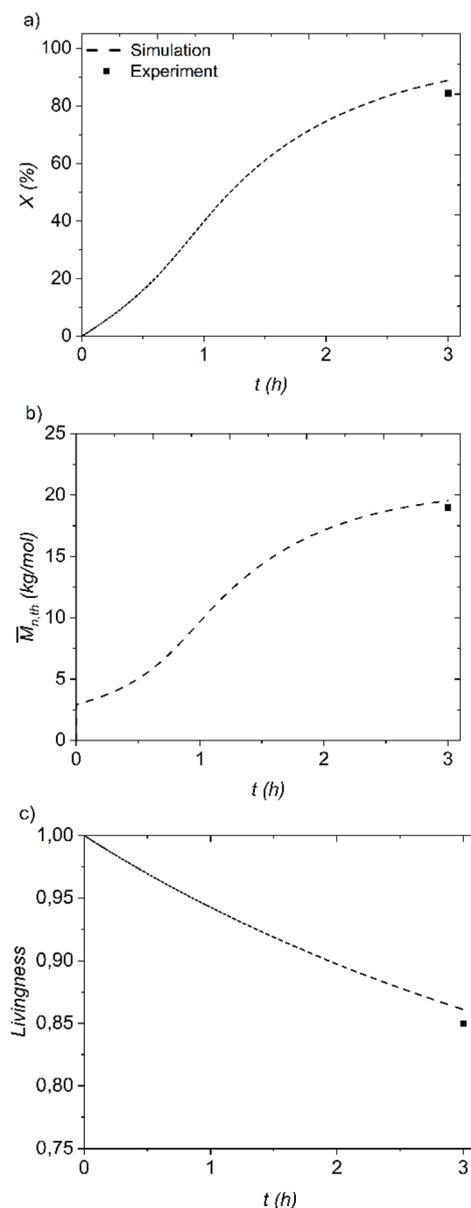

Fig. 8 Prediction of polymer synthesis characteristics from the reaction kinetic model with experimental validation. (a) Conversion of the DMAPAm monomer, (b) number average molar mass of PDMAPAm, and (c) livingness of PDMAPAm with polymerization time.

Table 1 Molecular characterization results of PDMAPAm and PDMA-PAm-*b*-PMMA obtained from GPC

Polymer	$\bar{M}_{n,app}$ (kDa)	$\bar{M}_{w,app}$ (kDa)	$Đ$
PDMAPAm$_{163}$	18.5	25.6	1.38
PDMAPAm$_{163}$-*b*-PMMA$_{30}$	20.4	29.3	1.44

Langmuir physisorption model) can be applied to determine the kinetic parameters of adsorption, such as q_{max} and k_L, and the CO_2 adsorption isotherm of PDMAPAm-*b*-PMMA can be predicted. To prove whether the prediction by both Langmuir models is right, the dry CO_2 adsorption isotherms of the PDMAPAm-*b*-PMMA diblock copolymer and PDMAPAm homopolymer were experimentally measured and compared with the simulated adsorption isotherm shown in Fig. 9.

It is clear from both curves that the dry CO_2 adsorption model accurately predicts the uptake capacity of the polymer, indicating that the physisorption model works correctly. In the dry CO_2 adsorption case, there is a small deviation in the simulated isotherm from the experimental result, but it starts from a pressure of 5 bar, which is not as relevant to direct air capture because these polymers are planned to be applied at atmospheric pressure in DAC.

While the laboratory methodology developed in this study involves detailed kinetic modeling, polymer synthesis optimization, and membrane-adsorber characterization, the underlying workflow is highly scalable because each step aligns with established industrial practices in membrane manufacturing and polymer processing.[137] The unified kinetic model offers a predictive design tool that reduces development time at the commercial scale by minimizing experimental trial-and-error during material selection and process optimization.[138] Furthermore, the scalability of RAFT polymerization and membrane-fabrication techniques such as phase inversion or coating ensures that the materials described herein can be produced at industrially relevant throughputs.[139] The ability to tailor the polymer composition digitally before synthesis contributes to significant cost savings by reducing raw-material waste, shortening development cycles, and enabling more sustainable manufacturing routes.[140] Overall,
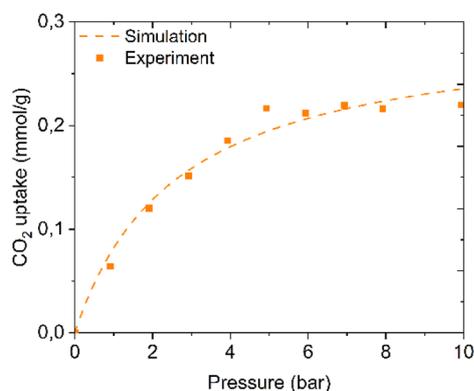
the methodology supports commercial deployment by coupling material-level optimization with process efficiency, and its potential economic impact is aligned with global incentives for carbon-capture technologies and emerging climate-policy frameworks.[141]

Conclusion

This study provides a comprehensive investigation into the CO_2 capture behavior of the CO_2-responsive homopolymer PDMAPAm and its diblock copolymer PDMAPAm-*b*-PMMA, with a focus on their applicability as membrane adsorbers for direct air capture (DAC) technologies. Under dry conditions, CO_2 was found to undergo physisorption, interacting primarily with the tertiary amine groups of PDMAPAm and the carbonyl functionalities of PMMA. This behavior was validated through gravimetric adsorption measurements, with the uptake capacities benchmarked against the existing literature.

Beyond mechanistic characterization, this study explored the kinetics of CO_2 adsorption and polymerization, incorporating physisorption pathways and polymerization kinetics into a unified model. This kinetic framework was integrated with polymerization kinetics to enable the rational design and optimization of the polymer properties. By varying the molar mass of the PDMAPAm block and the relative PMMA content, the influence of polymer composition on CO_2 uptake was systematically assessed. This approach allowed for the identification of the most effective polymer architecture for DAC applications, balancing adsorption capacity with material property. Notably, the unified model predicted a target molar mass of 18.5 kDa for the PDMAPAm$_{163}$ homopolymer and identified an optimal synthesis recipe of RAFT : initiator : monomer ratio of 1.2 : 1 : 200, corresponding to a polymerization time of 3 hours. The model also accurately forecasts the CO_2-uptake capacity of the PDMAPAm$_{163}$ homopolymer to be 0.05 mmol g^{-1} and that of the corresponding diblock copolymer (PDMAPAm$_{163}$-*b*-PMMA$_{30}$) to be approximately 0.1 mmol g^{-1} under dry ambient conditions.

Additionally, the impact of key process variables including temperature and pressure on CO_2 capture performance was thoroughly examined. The optimal operating conditions were determined, providing valuable guidance for the deployment of these materials in real-world DAC systems.

In summary, this work not only advances the understanding of CO_2-responsive polymer adsorption mechanisms but also establishes a robust framework for optimizing polymer design and process conditions. The findings underscore the promise of PDMAPAm-based materials in addressing the urgent need for effective DAC solutions and contribute to the broader efforts to mitigate atmospheric CO_2 levels through innovative materials science.

Looking ahead, adsorption-based carbon removal will increasingly rely on materials that combine high CO_2 uptake, low regeneration energy, and long-term cyclability under realistic atmospheric conditions. For PDMAPAm-based polymer membrane adsorbers, future research should focus on evaluating their performance under humid and variable-temperature environments, where the adsorption pathways or cooperative

Fig. 9 Comparison of the kinetic model prediction with the experimental results for dry CO_2 adsorption isotherm on the PDMAPAm$_{163}$-*b*-PMMA$_{30}$ diblock copolymer.

effects may further enhance their uptake. Integrating these materials into scalable membrane-adsorber modules, supported by techno-economic analysis and accelerated aging studies, will be essential to assess their practical viability in DAC operations. In parallel, expanding the unified kinetic model to include humidity-dependent equilibria, transport limitations, and multicomponent gas effects would provide a more predictive framework for guiding polymer design. Together, these efforts will help bridge the gap between laboratory-scale materials development and deployable DAC technologies.

Conflicts of interest

The authors declare no conflict of interest.

Data availability

All data supporting this study are provided in the supplementary information (SI) and previously published datasets. Supplementary information: includes details such as the synthesis procedure, structural characterization, theoretical calculations, experimental methods, and spectral analyses. For access to the datasets, refer to DOI: https://www.doi.org/10.5281/zenodo.17959928. See DOI: https://doi.org/10.1039/d5ta10366e.

Acknowledgements

References

1 M. Bui, C. S. Adjiman, A. Bardow, E. J. Anthony, A. Boston, S. Brown, P. S. Fennell, S. Fuss, A. Galindo and L. A. Hackett, *Energy Environ. Sci.*, 2018, **11**, 1062–1176.

2 C. M. White, B. R. Strazisar, E. J. Granite, J. S. Hoffman and H. W. Pennline, *J. Air Waste Manage. Assoc.*, 2003, **53**, 645–715.

3 P. C. Psarras, S. Comello, P. Bains, P. Charoensawadpong, S. Reichelstein and J. Wilcox, *Environ. Sci. Technol.*, 2017, **51**, 11440–11449.

4 X. Wang and C. Song, *Front. Energy Res.*, 2020, **8**, 560849.

5 M. Erans, E. S. Sanz-Pérez, D. P. Hanak, Z. Clulow, D. M. Reiner and G. A. Mutch, *Energy Environ. Sci.*, 2022, **15**, 1360–1405.

6 X. Zhu, W. Xie, J. Wu, Y. Miao, C. Xiang, C. Chen, B. Ge, Z. Gan, F. Yang and M. Zhang, *Chem. Soc. Rev.*, 2022, **51**, 6574–6651.

7 L. Küng, S. Aeschlimann, C. Charalambous, F. McIlwaine, J. Young, N. Shannon, K. Strassel, C. N. Maesano, R. Kahsar and D. Pike, *Energy Environ. Sci.*, 2023, **16**, 4280–4304.

8 J. Kotowicz, K. Niesporek and O. Baszczeńska, *Energies*, 2025, **18**, 496.

9 P. Webb, H. Muslemani, M. Fulton and N. Curson, *Scaling Direct Air Capture (DAC): A Moonshot or the Sky's the Limit?*, OIES Paper, CM, 2023.

10 Y. Zhang, J. Feng, L. Li, S. Zhao, C. Wu, Z. Huang and H. Lin, *Front. Energy*, 2025, 1–13.

11 D. Panda, V. Kulkarni and S. K. Singh, *React. Chem. Eng.*, 2023, **8**, 10–40.

12 J. Young, F. Mcilwaine, B. Smit, S. Garcia and M. Van der Spek, *Chem. Eng. J.*, 2023, **456**, 141035.

13 U. I. Premadasa, N. Kumar, D. Stamberga, V. Bocharova, J. T. Damron, T. Li, S. Roy, Y.-Z. Ma, V. S. Bryantsev and B. Doughty, *J. Chem. Phys.*, 2024, **161**, 164707.

14 J. Serafin and B. Dziejarski, *Microporous Mesoporous Mater.*, 2023, **354**, 112513.

15 S. Deutz and A. Bardow, *Nat. Energy*, 2021, **6**, 203–213.

16 A. Ward, M. M. Papathanasiou and R. Pini, *Adsorption*, 2024, **30**, 1829–1848.

17 K. An, K. Li, C.-M. Yang, J. Brechtl and K. Nawaz, *J. CO$_2$ Util.*, 2023, **76**, 102587.

18 M. Soukri, P. Sitaula, D. O'Nolan, M. G. Izenson and S. D. Phillips, *Development of Advanced Solid Sorbents for Direct Air Capture*, RTI International, Research Triangle Park, NC (United States), 2023.

19 C. Zhang, J. Fang, X. Xu, M. Zhang, Z. Han and J. Liao, *Ann. N. Y. Acad. Sci.*, 2025, **1552**, 388–400.

20 D. Li, S. Ning, L. Yu, F. Jiang, D. Zhao, S. Zhang, M. Liao, Q. Meng, Q. Fang and H. Kang, *Adv. Mater.*, 2025, 2501622.

21 G. Zhao, H. Gao, Z. Qu, H. Fan and H. Meng, *Nat. Commun.*, 2023, **14**, 7624.

22 X. Ju, X. Feng, X. Duan, B. Cui, G. Huang, Y. Chen, X. Tong, Z. Yang, P. Guo and S. Xu, *Sep. Purif. Technol.*, 2025, 136443.

23 F. Yan, H. Chen, T. Chi, J. Lu, X. Shen, F. Xie, P. Wang and Z. Zhang, *Chem. Eng. J.*, 2025, 166450.

24 X. Li, J. Yu, H. He, Z. Peng, J. Pu, L. Zheng, A. Chen, J. Qian, F. Huang and X. Gu, *Langmuir*, 2025, **41**, 29180–29195.

25 L. B. Hamdy, C. Goel, J. A. Rudd, A. R. Barron and E. Andreoli, *Mater. Adv.*, 2021, **2**, 5843–5880.

26 R. B. Said, J. M. Kolle, K. Essalah, B. Tangour and A. Sayari, *ACS Omega*, 2020, **5**, 26125–26133.

27 R. Zhang and J. Zhou, *Clean Energy Sci. Technol.*, 2024, **2**, 126.

28 E. Wang, R. Navik, Y. Miao, Q. Gao, D. Izikowitz, L. Chen and J. Li, *Cell Rep. Phys. Sci.*, 2024, 101791.

29 Z. Wan, R. Hunt, C. White, J. Gillbanks, J. Czapla, G. Xiao, S. Surin and C. Wood, *ChemSusChem*, 2024, e202400212.

30 S. H. Pang, R. P. Lively and C. W. Jones, *ChemSusChem*, 2018, **11**, 2628–2637.

31 K. Li, J. Jiang, F. Yan, S. Tian and X. Chen, *Appl. Energy*, 2014, **136**, 750–755.

32 C. Zhang, J. Zhou, X. Ye, Z. Li and Y. Wang, *J. Membr. Sci.*, 2022, **641**, 119928.

33 M.-S. Lebrun-Chopra, *The Development of Novel Bio-Based CO₂-Responsive Polymers for Binder Applications*, Queen's University, Canada, 2021.

34 Y.-T. Shieh, Y.-T. Lin and C.-C. Cheng, *Carbohydr. Polym.*, 2017, **170**, 281–288.

35 K. Bauri, A. Pan, U. Haldar, A. Narayanan and P. De, *J. Polym. Sci., Part A: Polym. Chem.*, 2016, **54**, 2794–2803.

36 A. Riabtseva, S. N. Ellis, P. Champagne, P. G. Jessop and M. F. Cunningham, *Ind. Eng. Chem. Res.*, 2021, **60**, 9807–9816.

37 M. F. Cunningham and P. G. Jessop, *Macromol. React. Eng.*, 2022, **16**, 2200031.

38 M. F. Cunningham and P. G. Jessop, *Chem. Commun.*, 2023, **59**, 13272–13288.

39 M. F. Cunningham and P. G. Jessop, *Eur. Polym. J.*, 2016, **76**, 208–215.

40 W. Ji, D. Panus, R. N. Palumbo, R. Tang and C. Wang, *Biomacromolecules*, 2011, **12**, 4373–4385.

41 S. Demirci, S. D. Sutekin, O. Guven and N. Sahiner, *Int. J. Hydrogen Energy*, 2023, **48**, 23002–23012.

42 E. Pashayev, F. Kandelhard and P. Georgopanos, *Macromol. React. Eng.*, 2023, **17**, 2200068.

43 R. Du, A. Chakma and X. Feng, *J. Membr. Sci.*, 2007, **290**, 19–28.

44 Z. Zhou, T. Liu, A. U. Khan and G. Liu, *Sci. Adv.*, 2019, **5**, eaau6852.

45 A. Esmeraldo Paiva, J. F. Baez Vasquez, A. Selkirk, N. Prochukhan, F. GL Medeiros Borsagli and M. Morris, *ACS Appl. Mater. Interfaces*, 2022, **14**, 35265–35275.

46 K. Nieswandt, P. Georgopanos and V. Abetz, *Polym. Chem.*, 2021, **12**, 2210–2221.

47 R. Shevate, M. Kumar, M. Karunakaran, C. Canlas and K.-V. Peinemann, *J. Mater. Chem. A*, 2018, **6**, 4337–4345.

48 L. Tsaur and U. B. Wiesner, *Polymers*, 2023, **15**, 2020.

49 F. Kandelhard, K. Schuldt, J. Schymura, P. Georgopanos and V. Abetz, *Macromol. React. Eng.*, 2021, **15**, 2000058.

50 F. Kandelhard, E. Pashayev, J. Schymura and P. Georgopanos, *Ind. Eng. Chem. Res.*, 2023, **62**, 8696–8708.

51 E. Pashayev and P. Georgopanos, *Macromol. Mater. Eng.*, 2025, **310**, 2400290.

52 T. Tiainen, J. K. Mannisto, H. Tenhu and S. Hietala, *Langmuir*, 2021, **38**, 5197–5208.

53 S. Lin and P. Theato, *Macromol. Rapid Commun.*, 2013, **34**, 1118–1133.

54 M. Zhao, L. Huang, Y. Gao, Z. Wang, S. Liang, X. Zhu, Q. Wang, H. He and D. O'Hare, *Nano-Micro Lett.*, 2025, **17**, 1–19.

55 J. Y. Bae, S. G. Jang, J. Cho and M. Kang, *Int. J. Mol. Sci.*, 2025, **26**, 4313.

56 B. Zhang, C. Zheng, F. S. Bates and T. P. Lodge, *ACS Appl. Polym. Mater.*, 2023, **5**, 2223–2229.

57 D. J. Lohse and N. Hadjichristidis, *Curr. Opin. Colloid Interface Sci.*, 1997, **2**, 171–176.

58 E. Pashayev and P. Georgopanos, *Chem. Ing. Tech.*, 2025, **97**, 703–709.

59 R. W. Baker, *Membrane Technology and Applications*, John Wiley & Sons, 2023.

60 Y. Chen, K.-J. Lu, S. Japip and T.-S. Chung, *Environ. Sci. Technol.*, 2020, **54**, 12713–12722.

61 K. Sumida, D. L. Rogow, J. A. Mason, T. M. McDonald, E. D. Bloch, Z. R. Herm, T.-H. Bae and J. R. Long, *Chem. Rev.*, 2012, **112**, 724–781.

62 G. Firpo, E. Angeli, P. Guida, D. Pezzuoli, D. Repetto, L. Repetto and U. Valbusa, *Polymers*, 2019, **11**, 910.

63 J. Zhou, M. Deissenroth-Uhrig and M. Gallei, *Adv. Funct. Mater.*, 2025, e20959.

64 A. K. Sekizkardes, P. Wang, J. Hoffman, S. Budhathoki and D. Hopkinson, *Mater. Adv.*, 2022, **3**, 6668–6686.

65 H. Liu, H. Yin and Y. Feng, *Des. Monomers Polym.*, 2017, **20**, 363–367.

66 A. L. Krasovskiy, E. Auyeung, B. D. Stubbert, A. V. Davis, J. Hou and C. H. Cummins, Process for preparing olefin-acrylate block copolymers, WO2021222694A1, 2023.

67 E. Pashayev and P. Georgopanos, *Polymers*, 2025, **17**, 1115.

68 G. Desmet, N. Rybel and P. Steenberge, *Macromol. Rapid Commun.*, 2017, **39**, 1700403.

69 A. Spiteri, B. Megerle, A. Calbry-Muzyka, N. Casas and J. A. Wurzbacher, Method for capture of carbon dioxide from ambient air and corresponding adsorber structures with a plurality of parallel surfaces, WO2021239747A1, 2023.

70 S. M. Lalji, M. Ayubi, S. I. Ali, S. u. Rahman and M. Mustafa, *Discov. Chem.*, 2024, **1**, 71.

71 Q. Grossmann, P. A. Saenz-Cavazos, N. Ferru, D. R. Williams and M. Mazzotti, *Ind. Eng. Chem. Res.*, 2025, **64**, 7165–7175.

72 R. P. S. Gautam and S. Sahoo, *Sādhanā*, 2023, **48**, 27.

73 M. O. Prache, *Institutt for Kjemisk Prosessteknologi*, 2012.

74 J. Hwang, H. Azzan, R. Pini and C. Petit, *J. Chem. Eng. Data*, 2022, **67**, 1674–1686.

75 X. Yang, R. Kleinrahm, M. O. McLinden and M. Richter, *Int. J. Thermophys.*, 2023, **44**, 169.

76 Q. Li, X. He, Y. Cui, P. Shi, S. Li and W. Zhang, *Polym. Chem.*, 2015, **6**, 70–78.

77 Q.-l. Li, L. Li, H.-s. Wang, R. Wang, W. Wang, Y.-j. Jiang, Q. Tian and J.-p. Liu, *Chin. J. Polym. Sci.*, 2017, **35**, 66–77.

78 Q. Li, L. Li, W. Wang, X. Zhang, S. Li, Q. Tian and J. Liu, *RSC Adv.*, 2016, **6**, 45305–45314.

79 F. Monemian and A. Kargari, *J. Polym. Environ.*, 2025, **33**, 4921–4941.

80 E. Orestes, C. M. Ronconi and J. W. de Mesquita Carneiro, *Phys. Chem. Chem. Phys.*, 2014, **16**, 17213–17219.

81 M. Haris, A. Aziz, M. Sohail and W. Sardar, *Environ. Sci. Pollut. Res.*, 2025, 1–19.

82 S. Zulfiqar, M. I. Sarwar and C. T. Yavuz, *RSC Adv.*, 2014, **4**, 52263–52269.

83 M. N. Khan, Y. van Ingen, T. Boruah, A. McLauchlan, T. Wirth and R. L. Melen, *Chem. Sci.*, 2023, **14**, 13661–13695.

84 R. Wissinger and M. Paulaitis, *J. Polym. Sci., Part B:Polym. Phys.*, 1987, **25**, 2497–2510.

85 J. Kim, K. H. Kim, Y. Ryu and S. W. Cha, *Polymers*, 2022, **14**, 596.

86 R. G. Wissinger and M. E. Paulaitis, *Ind. Eng. Chem. Res.*, 1991, **30**, 842–851.

87 J. H. Aubert, *J. Supercrit. Fluids*, 1998, **11**, 163–172.

88 D. Liu, H. Li, M. S. Noon and D. L. Tomasko, *Macromolecules*, 2005, **38**, 4416–4424.

89 K. F. Webb and A. S. Teja, *Fluid Phase Equilib.*, 1999, **158**, 1029–1034.

90 E. Kiran, J. A. Sarver and J. C. Hassler, *J. Supercrit. Fluids*, 2022, **185**, 105378.

91 J. Fried and W. Li, *J. Appl. Polym. Sci.*, 1990, **41**, 1123–1131.

92 M. R. Nelson and R. F. Borkman, *J. Phys. Chem. A*, 1998, **102**, 7860–7863.

93 Y.-T. Shieh and K.-H. Liu, *J. Supercrit. Fluids*, 2003, **25**, 261–268.

94 M. Takahashi, Y. Yamamoto, A. V. Nawaby and Y. P. Handa, *J. Polym. Sci., Part B:Polym. Phys.*, 2003, **41**, 2214–2217.

95 Y.-T. Shieh and K.-H. Liu, *J. Polym. Res.*, 2002, **9**, 107–113.

96 E. Ricci, M. G. De Angelis and M. Minelli, *Chem. Eng. J.*, 2022, **435**, 135013.

97 M. A. Blatchford, P. Raveendran and S. L. Wallen, *J. Phys. Chem. A*, 2003, **107**, 10311–10323.

98 Y. G. Ko, S. S. Shin and U. S. Choi, *J. Colloid Interface Sci.*, 2011, **361**, 594–602.

99 P. Bollini, S. Choi, J. H. Drese and C. W. Jones, *Energy Fuels*, 2011, **25**, 2416–2425.

100 K. Inkong, P. Rangsunvigit, T. Chaisuwan and S. Kulprathipanja, *Chem. Eng. Trans.*, 2016, **52**, 103–108.

101 C. Pornjariyawatch, V. Jitchum, K. Assawatwikrai, P. Leepakorn, M. Probst, B. Boekfa, T. Maihom and J. Limtrakul, *ChemPhysChem*, 2025, **26**, e202400754.

102 W. Jiang, Y. Lin, C. Sun, Y. Sun and Y. Zhu, *Molecules*, 2024, **29**, 4618.

103 X. Sun, X. Shen, H. Wang, F. Yan, J. Hua, G. Li and Z. Zhang, *Nat. Commun.*, 2024, **15**, 5068.

104 J. Hack, N. Maeda and D. M. Meier, *ACS Omega*, 2022, **7**, 39520–39530.

105 S. Lin, K. R. Storme, Y.-C. M. Wu, F. M. Benedetti, T. M. Swager and Z. P. Smith, *J. Membr. Sci.*, 2023, **668**, 121194.

106 F. M. Benedetti, Y.-C. M. Wu, S. Lin, Y. He, E. Flear, K. R. Storme, C. Liu, Y. Zhao, T. M. Swager and Z. P. Smith, *JACS Au*, 2022, **2**, 1610–1615.

107 M. Ciulla, V. Canale, R. Wolicki, S. Pilato, P. Bruni, S. Ferrari, G. Siani, A. Fontana and P. Di Profio, *Separations*, 2023, **10**, 505.

108 C. Li, D. Lu and C. Wu, *Phys. Chem. Chem. Phys.*, 2020, **22**, 11354–11361.

109 T. Xu, Z. Wang, T. Liu, F. Wang and Y. Jing, *J. Am. Chem. Soc.*, 2025, **147**, 26969–26979.

110 R. Navik, E. Wang, X. Ding, K. Qiu and J. Li, *Environ. Chem. Lett.*, 2024, **22**, 1791–1830.

111 P. Singh, J. P. Niederer and G. F. Versteeg, *Chem. Eng. Res. Des.*, 2009, **87**, 135–144.

112 X. Deng, Y. Han, L.-C. Lin and W. W. Ho, *Sep. Purif. Technol.*, 2022, **299**, 121601.

113 S. Kilic, S. Michalik, Y. Wang, J. K. Johnson, R. M. Enick and E. J. Beckman, *Macromolecules*, 2007, **40**, 1332–1341.

114 S. Kilic, S. Michalik, Y. Wang, J. Johnson, R. Enick and E. Beckman, *Ind. Eng. Chem. Res.*, 2003, **42**, 6415–6424.

115 H. Schellevis, J. De La Combé and D. Brilman, *Energy Adv.*, 2024, **3**, 1678–1687.

116 X. Cai, M. A. Coletti, D. S. Sholl and M. R. Allen-Dumas, *JACS Au*, 2024, **4**, 1883–1891.

117 A. A. Al-Absi, A. Domin, M. Mohamedali, A. M. Benneker and N. Mahinpey, *Fuel*, 2023, **333**, 126401.

118 M. Mabuza, K. Premlall and M. O. Daramola, *Int. J. Coal Sci. Technol.*, 2022, **9**, 45.

119 B. Dziejarski and A. Kisiela-Czajka, *Mach., Technol., Mater.*, 2021, **15**, 299–302.

120 M. Jiang, J. Wang, L. Li, K. Pan and B. Cao, *RSC Adv.*, 2013, **3**, 20625–20632.

121 S. Fan, J. Chen, C. Fan, G. Chen, S. Liu, H. Zhou, R. Liu, Y. Zhang, H. Hu and Z. Huang, *J. Hazard. Mater.*, 2021, **416**, 126225.

122 J. Qu, L. Chang, M. Liu, B. Cao, M. Li, Q. Yang and W. Gong, *Polymers*, 2022, **14**, 4187.

123 I. Langmuir, *J. Am. Chem. Soc.*, 1916, **38**, 2221–2295.

124 I. Langmuir, *J. Am. Chem. Soc.*, 1918, **40**, 1361–1403.

125 S. Kundu and A. K. Gupta, *Chem. Eng. J.*, 2006, **122**, 93–106.

126 K. Vijayaraghavan, T. Padmesh, K. Palanivelu and M. Velan, *J. Hazard. Mater.*, 2006, **133**, 304–308.

127 D. R. Paul, *Polymeric Gas Separation Membranes*, CRC press, 2018.

128 G. K. V. Saraiva, V. V. de Souza, L. C. de Oliveira, M. L. d. C. Noronha, J. C. Masini, H. Chaimovich, R. K. Salinas, F. H. Florenzano and I. M. Cuccovia, *Colloid Polym. Sci.*, 2019, **297**, 557–569.

129 X. Han, N. Gong, X. Si, C. Jiang, J. Xu, S. Sun, P. Zhan and J. Mu, *J. Polym. Res.*, 2023, **30**, 223.

130 F. Li, M. Schellekens, J. de Bont, R. Peters, A. Overbeek, F. A. Leermakers and R. Tuinier, *Macromolecules*, 2015, **48**, 1194–1203.

131 A. Khaydarov, I. W. Hamley, T. M. Legge and S. Perrier, *Eur. Polym. J.*, 2007, **43**, 789–796.

132 M. A. Otmi, F. Willmore and J. Sampath, *Macromolecules*, 2023, **56**, 9042–9053.

133 A. F. Ismail, T. D. Kusworo, A. Mustafa and H. Hasbulla, *Understanding the Solution-Diffusion Mechanism in Gas Separation Membrane for Engineering Students*, 2005.

134 T. Corrado and R. Guo, *Mol. Syst. Des. Eng.*, 2020, **5**, 22–48.

135 R. K. Arya, D. Thapliyal, J. Sharma and G. D. Verros, *Coatings*, 2021, **11**, 1049.

136 N. Berrahou, A. Mokaddem, B. Doumi, S. Hiadsi, N. Beldjoudi and A. Boutaous, *Polym. Bull.*, 2016, **73**, 3007–3017.

137 S. H. Alkandari and B. Castro-Dominguez, *Front. Membr. Sci. Technol.*, 2024, **3**, 1390599.

138 M. Gaulke, V. Guschin, S. Knapp, S. Pappert and W. Eckl, *Microporous Mesoporous Mater.*, 2016, **233**, 39–43.

139 S. Perrier, *Macromolecules*, 2017, **50**, 7433–7447.

140 U. Han, T. Kang, J. Im and J. Hong, *Chem. Commun.*, 2022, **58**, 10953–10956.

141 M. Ho, V. Barahimi and E. Croiset, *The State of Direct Air Capture Technology and Industry, Waterloo Climate Institute*, University of Waterloo, Waterloo, Ontario, Canada, 2025.